Cerebral Cortex, June 2019;29: 2728–2736

doi: 10.1093/cercor/bhy142
Advance Access Publication Date: 25 May 2018
Original Article

ORIGINAL ARTICLE

Differential Contributions of Glutamatergic Hippocampal→Retrosplenial Cortical Projections to the Formation and Persistence of Context Memories

Naoki Yamawaki[1], Kevin A. Corcoran[2], Anita L. Guedea[2], Gordon M.G. Shepherd[1] and Jelena Radulovic[1,2]

[1]Department of Physiology, Northwestern University, Feinberg School of Medicine, Chicago, IL 60611, USA and [2]Department of Psychiatry and Behavioral Sciences, Northwestern University, Feinberg School of Medicine, Chicago, IL 60611, USA

Address correspondence to Jelena Radulovic, Northwestern University, Feinberg School of Medicine, 303 E Chicago Ave, Ward 13-130, Chicago, IL 60611, USA. Email: j-radulovic@northwestern.edu

Abstract

Learning to associate stressful events with specific environmental contexts depends on excitatory transmission in the hippocampus, but how this information is transmitted to the neocortex for lasting memory storage is unclear. We identified dorsal hippocampal (DH) projections to the retrosplenial cortex (RSC), which arise mainly from the subiculum and contain either the vesicular glutamate transporter 1 (vGlut1) or vGlut2. Both vGlut1$^+$ and vGlut2$^+$ axons strongly excite and disynaptically inhibit RSC pyramidal neurons in superficial layers, but vGlut2$^+$ axons trigger greater inhibition that spreads to deep layers, indicating that these pathways engage RSC circuits via partially redundant, partially differentiated cellular mechanisms. Using contextual fear conditioning in mice to model contextual associative memories, together with chemogenetic axonal silencing, we found that vGlut1$^+$ projections are principally involved in processing recent context memories whereas vGlut2$^+$ projections contribute to their long-lasting storage. Thus, within the DH→RSC pathway, engagement of vGlut1$^+$ and vGlut2$^+$ circuits differentially contribute to the formation and persistence of fear-inducing context memories.

Key words: context fear conditioning, hippocampus, retrosplenial cortex, vGlut1, vGlut2

Introduction

Episodic memories contain details of past events, including where they occurred. The hippocampus, and in particular its posterior (dorsal in rodents) subdivision, is critical for the formation of episodic memories, whereas its interactions with the cortex are believed to provide a foundation for lasting memory storage through a process termed systems consolidation (Squire and Alvarez 1995). Understanding the mechanisms underlying these interactions will further our knowledge of basic principles of memory but also provide novel targets for memory disorders, which range from impairments (dementia) to excessive persistence (post-traumatic stress disorder) of episodic memories.

In animal models, learning to associate stressful events with specific environmental contexts can be rapidly induced by contextual fear conditioning (CFC). In CFC, exposure to a context is terminated with brief footshock, resulting in a context/shock association and context-specific freezing upon re-exposure to the context (Blanchard and Blanchard 1969; Fanselow 1990). To date, several neocortical areas have been implicated in the long-term processing of fear-inducing context memories including the anterior cingulate (Frankland et al. 2004; Wiltgen and Tanaka 2013), retrosplenial [RSC, (Corcoran et al. 2011)], and medial prefrontal (Kitamura et al. 2017) cortices. Of these areas, dorsal hippocampal (DH) projects directly only to RSC (Cenquizca and Swanson 2007).

Moreover, glutamatergic neurotransmission in DH and RSC is required for CFC (Keene and Bucci 2008; Gao et al. 2010; Corcoran et al. 2011; Cowansage et al. 2014; Kwapis et al. 2014). Interestingly, RSC activity is required for processing of both recent and remote memories (Corcoran et al. 2011), suggesting that DH→RSC projections transmit essential contextual information required for cortical memory processing from the early stages of stimulus encoding (Van Groen and Wyss 2003; Aggleton 2010).

To provide experimental support for this assumption, we sought to understand in more depth the cellular and circuit mechanisms underlying DH-RSC interactions, and to determine their contributions to storage and retrieval of fear-inducing context memories. We show that vGlut1$^+$ and vGlut2$^+$ neuronal populations in the DH, predominantly localized in the SUB, project to the RSC and distinctively regulate RSC local cellular networks. Using chemogenetic silencing of DH→RSC terminals, we found a major role of vGlut1$^+$ projections in encoding and retrieval of recent context memory, whereas vGlut2$^+$ projections, on the other hand contributed to its persistence.

Materials and Methods

Animals

We used male and female C57BL/6J mice, vGlut1-Cre, and vGlut2-Cre male mice. Wild-type C57BL6/J mice were purchased from Harlan, Indianapolis, IN. The vGlut1-Cre mouse line, also known as Slc17a7-IRES2-Cre or Vglut1-IRES2-Cre-D, was created by the Hongkui Zeng lab, Allen Institute for Brain Science (Harris et al. 2014), and obtained from the Jackson Laboratory (Bar Harbor, ME). These knockin mice express Cre recombinase in vGlut1+ cells, without disrupting endogenous vGlut1 expression. Cre recombinase expression (performed with *in situ* hybridization using a Cre-specific probe) showed a pattern similar to that of the endogenous Slc17a7 gene (Allen Institute for Brain Science website Slc17a7-IRES2-Cre images), as also confirmed with our immunohistochemical analyses. The vGlut2-Cre knockin mice, also known as Slc17a6tm2(cre) and Lowl or VGlut2-ires-Cre, express Cre recombinase in excitatory glutamatergic neuron cell bodies, without disrupting endogenous vGlut2 expression, as described previously (Vong et al. 2011).

All mice were 8 weeks of age at the beginning of the experiments. The mice were maintained under standard housing conditions (12/12 h light dark cycle with lights on at 7 a.m., temperature 20–22 °C, humidity 30–60%) in our satellite behavioral facility. All animal procedures used in this study were approved by the Northwestern University IACUC and complied with federal regulations set forth by the National Institutes of Health.

Heterozygous vGlut1-Cre mice [Jackson 023527, strain of origin (129S6/SvEvTac x C57BL/6NCrl)F1, bred with C57BL/6 J wild-type mice for several generations in the Zeng laboratory and 3 generations at the Jackson Laboratory] were backcrossed with wild-type C57BL6/J for 6 generations in our facility to achieve offspring with a genetic identity which is closer to the C57BL6/J strain. The colony was subsequently expanded by homozygous breeding. Genotyping was confirmed by polymerase chain reaction (PCR) with 3 primers. The common (5′-ATG AGC GAG GAG AAG TGT GG-3′) and endogenous (5′-GTG GAA GTC CTG GAA ACT GC-3′) primers generate a 218-bp PCR product from the endogenous locus, while the common and mutant (5′-CCC TAG GAA TGC TCG TCA AG-3′) primers generate a 344-bp product from the targeted locus. Homozygous vGlut2-Cre (Jackson 016 963) mice were also backcrossed with wild-type C57BL6/J for 6 generations and the colony was expanded by homozygous breeding. Typically, we obtained 4–6 litters/breeding cycle with 5–8 mice/litter with similar distribution of males and females. All litters were used for behavioral experiments and randomly selected mice were used for tracing and electrophysiological studies. Genotyping was confirmed by PCR with 3 primers. The common (5′-AAG AAG GTG CGC AAG ACG-3′) and endogenous (5′-CTG CCA CAG ATT GCA CTT GA-3′) primers generate a 299-bp PCR product from the endogenous locus, while the common and mutant (5′-ACA CCG GCC TTA TTC CAA G-3′) primers generate a 850-bp product from the targeted locus.

Contextual Fear Conditioning

CFC was performed in an automated system (TSE Systems) as described previously (Corcoran et al. 2011). Briefly, mice were exposed for 3 min to a novel context, followed by a footshock (2 s, 0.7 mA, constant current). Mice were tested for memory retrieval 24 h later by returning them to the conditioning context for 3 min. Freezing was scored every 10 s during context exposures and expressed as a percentage of the total number of observations during which the mice were motionless. All behavioral experiments were performed between 10 a.m. and 2 p.m. Littermates were randomly assigned to the different treatment conditions. All behavioral tests and immunohistochemical analyses were performed by experimenters who were blind to genotypes and drug treatments.

Stereotaxic Surgeries and Infusions of Viral Vectors and Drugs

Mice were anesthetized with 1.2% tribromoethanol (vol/vol, Avertin) for viral vector intracranial infusion and cannula implantation. The viral vector carrying a construct coding for the Cre-independent inhibitory DREADD (AAV8-hSyn-HA-hM4D(Gi)-mCherry, Addgene 44 362) or Cre-dependent inhibitory DREADD (AAV8-hSyn-DIO-hM4D(Gi)-mCherry, Addgene 50 475) was bilaterally infused into the dorsal hippocampus (1.8 mm posterior, ±1.0 mm lateral, 2.25 mm ventral to bregma). Infusions were performed using an automatic microsyringe pump controller (Micro4-WPI) connected to a Hamilton microsyringe. The viral vectors were infused in a volume of 0.5 µL per site over 2 min, and syringes were left in place for 5 min prior to removal to allow for virus diffusion. Bilateral 26 gauge guide cannulas (Plastics One) were placed in RSC (1.7 mm posterior, ±0.4 mm lateral, 0.75 mm ventral to bregma). Mice were allowed 6 weeks for virus expression prior to behavioral testing. Clozapine-*N*-oxide (Sigma; 0.3 µg/mL; 0.20 µL per side, at a rate of 0.5 µL/min) was infused through the cannulas 30 min prior to either fear conditioning or memory retrieval testing. Bicuculline (Sigma) was infused under the same conditions at 3 doses (0.25 µg/µL, 0.5 µg/µL, and 1 µg/µL). After the completion of behavioral testing, all brains were collected and cannula placements and virus spread were confirmed by immunohistochemical analysis using anti-mCherry antibodies (1:1 000; Abcam, Ab167453). For retrograde tracing with hydroxystilbamidine (Fluoro-Gold, Fluorohrome) we infused 0.2 µL of a 4% Fluoro-Gold solution in artificial cerebrospinal fluid (aCSF) into RSC and 5 days later collected and perfused the brains in 4% paraformaldehyde.

Immunohistochemistry and Immunofluorescence

Mice were anesthetized with an i.p. injection of 240 mg/kg Avertin and transcardially perfused with ice-cold 4% paraformaldehyde in phosphate buffer (pH 7.4, 150 mL per mouse).

Brains were removed and postfixed for 48 h in the same fixative and then immersed for 24 h each in 20% and 30% sucrose in phosphate buffer. Brains was frozen and 50 μm sections were cut for use in free-floating immunohistochemistry (Jovasevic et al. 2015) with primary antibodies against vGlut1 (1:4000; Abcam AB104898), vGlut2 (1:2000; Millipore, Cat # MAB5504), mCherry (1:1000; Abcam AB167453), and Fluoro-Gold (Fluorochrome 1:40 000). Immunostaining with mCherry, vGlut1, vGlut2, and Fluoro-Gold antibodies was visualized with diaminobenzidine (Sigma), fluorescein isothiocyanate (TSA systems, excitation 494 nm, emission 517 nm) or tetramethylrhodamine (TSA systems, excitation 550 nm, emission 570 nm). Sections were mounted using Vectashield (Vector) and observed with a confocal laser-scanning microscope (Olympus Fluoview FV10i) at 40×. Areas of mCherry immunostaining (red) were identified, marked, and superimposed on vGlut2 images to determine colocalization.

Slice electrophysiology and Optogenetics

Mice were anesthetized with isoflurane and head-fixed on stereotaxic frame. Craniotomy was performed above SUB (from bregma, in mm: 2.4 posterior, 1.5 lateral) and a beveled glass pipette loaded with Cre-dependent virus encoding eGFP (AAV1-CAG-Flex-eGFP-WPRE-bGH, Upenn, AV-1-ALL854) or hChR2 (AAV5-EF1a-DIO-hChR2(E123T/T159C)-EYFP, Upenn, AV-5–35 509) was injected unilaterally into SUB (1.6-mm deep from surface) using a hydraulic displacement injector (Narishige MO-10). For experiments involving analysis of spiking properties, red RetroBeads (Lumafluor) were additionally injected into RSC (in mm: 1.6 posterior, 0.2 lateral). Furthermore, to label RSC-projecting vGlut1+ neurons, Cre-dependent retrograde AAV encoding tdTomato was injected into RSC of vGlut1-Cre mice (Fig. 2). After 3–5 weeks of viral expression, brain was removed and coronal slices (250 μm) containing RSC were prepared using a vibratome (Leica VT1200S) in ice-cold choline-based cutting solution containing (in mM): 25 $NaHCO_3$, 1.25 NaH_2PO_3, 2.5 KCl, 0.5 $CaCl_2$, 7 $MgCl_2$, 110 choline chloride, 11.6 sodium L-ascorbate, and 3.1 sodium pyruvate, aerated with 95% O_2 and 5% CO_2. Slices were subsequently stored in a holding chamber filled with aCSF containing (in mM): 127 NaCl, 25 D-glucose, 2.5 KCl, 1 $MgCl_2$, 2 $CaCl_2$, and 1.25 NaH_2PO_3, aired with 95% O_2 and 5% CO_2, at 34 °C for 30 min and then at room temperature (~21 °C) for at least 1 h before recording.

Electrophysiological recordings were performed using an upright microscope (BX51WI, Olympus) equipped with gradient-contrast and epifluorescence optics and a blue LED (M470L2, Thorlabs) for photostimulation. Whole-cell recordings were made using borosilicate glass pipettes (~4–6 MΩ). For circuit analysis, to measure excitatory postsynaptic currents (EPSCs) and inhibitory postsynaptic current (IPSCs) the pipette was filled with a cesium-based internal solution composed of (in mM): 128 cesium methanesulfonate, 10 HEPES, 10 phosphocreatine, 4 $MgCl_2$, 4 ATP, 0.4 GTP, 3 ascorbate, 1 EGTA, 1 mM QX-314, pH 7.25, 290–295 mOsm. To examine spike patterns, cesium methanesulfonate was replaced with potassium methanesulfonate. Photostimulation of ChR2-expressing axons was performed using 4× objective lens (UPlanSApo, N/A 0.16, Olympus) focused on the slice, by briefly (5 ms) gating an output of blue LED (1.00 mW/mm^2 intensity in the specimen plane). To measure photo-evoked synaptic input, recordings were performed in voltage-clamp mode. The command potential was set to −70 mV (the approximate reverse potential of GABAergic current) to record EPSCs, then to 0–10 mV (the approximate reverse potential of glutamatergic current) to measure IPSCs. In one neuron, only EPSCs were recorded. Responses to multiple trials were sampled with an interstimulus interval of 20 s. Recordings with series resistance above 40 MΩ were discarded. Data were acquired and hardware was controlled using Ephus software (Suter et al. 2010). Signals were amplified using Axon Multiclamp 400B (Molecular Devices), filtered at 4 kHz, and sampled at 10 kHz. Traces were analyzed using Matlab routines. Photo-evoked EPSCs or IPSCs from multiple trials in each neuron were averaged and the response was computed as the mean current over a poststimulus interval of 50 ms. For comparison of DH input to superficial and deep layers of RSC, responses recorded from each neuron in the same slice were normalized to mean responses of all recorded neurons. Data were then pooled into superficial and deep layers based on position of the soma relative to the border of layers 3 and 5 A. Relative to EPSCs, the IPSCs were much larger in amplitude (reflecting the increased driving force for inhibitory conductances), and slightly slower in onset (by 2.6 ms on average, reflecting the disynaptic activation of the inhibitory responses), as expected for this method of sampling EPSCs and IPSCs in the same neuron by voltage manipulations (e.g., Apicella et al. 2012; Xue et al. 2014).

For spike pattern analysis, whole-cell recordings were performed from $vGlut1^+$ or $vGlut2^+$ RSC-projecting neurons identified by co-labeling of eGFP and red Retrobeads. After 3 min from break in, current steps (from −200 to 800 pA at 100 pA increment) were injected into the soma. The voltage traces obtained at the threshold response were analyzed offline to measure interspike intervals.

To test the effectiveness of hM4D(Gi) in silencing synaptic transmission in slices, AAV8-DIO-hM4D(Gi) and AAV5-DIO-hChR2 were infused into DH of either vGlut1- or vGlut2-Cre mice via cannula. The infusion of hM4D(Gi) preceded that of hChR2 by 3 weeks, and 3 more weeks were then allowed for viral expression; thus, hM4D(Gi) was expressed for 6 weeks to be consistent with expression time used in behavioral experiments. RSC slices were then prepared, and whole-cell recordings were made from layer 3 pyramidal neurons. Photostimuli were delivered every 30 s to depolarize $vGlut1^+$ or $vGlut2^+$ DH terminals, evoking excitatory synaptic transmission detected as EPSCs in the recorded postsynaptic neuron. After 5 min of stable baseline recording, clozapine-*N*-oxide (CNO) (0.03 μM or 0.1 μM) was bath-applied and recording was continued for at least 5 min. As a control, separate groups of mice from each Cre-line were injected with only ChR2 into DH using a glass pipette, and same slice experiment was repeated. A 1 mM stock of CNO solution was made daily before its bath application from powder (Sigma-Aldech, C0832-5MG) using H_2O as a solvent. Data were normalized to the mean baseline to assess the time-dependent effect of CNO at each concentration. To compare pre- and post-CNO EPSCs, traces from 1 min immediately before and the fifth minute after CNO (0.1 μM) application was averaged, and 50 ms mean current over a poststimulus interval of 50 ms was calculated.

Quantification and Statistical Analyses

Statistical analyses were performed using SPSS software and Matlab functions. For the behavioral studies, context freezing data were analyzed for treatment (CNO or Veh) as a factor using 2-tailed Student's *t* tests. Significant *F* values were followed by post hoc comparisons using Tukey's test. Homogeneity of variance was confirmed with Levene's test for equality of variances. Statistical differences were considered significant for all *P* values <0.05. Group sizes were determined using power

analyses assuming a moderate effect size of 0.5. All key findings were replicated at least twice.

Details of statistical analyses are found in figure legends. All source data for the preparation of graphs and statistical analysis are presented online. All other relevant data that support the conclusions of the study are available from the authors upon request.

Results

Chemogenetic Silencing of DH→RSC Terminals Impairs Memory Encoding of CFC

To determine the functional role of DH→RSC projections in CFC we used a chemogenetic approach with the inhibitory Designer Receptors Exclusively Activated by Designer Drugs (DREADD)

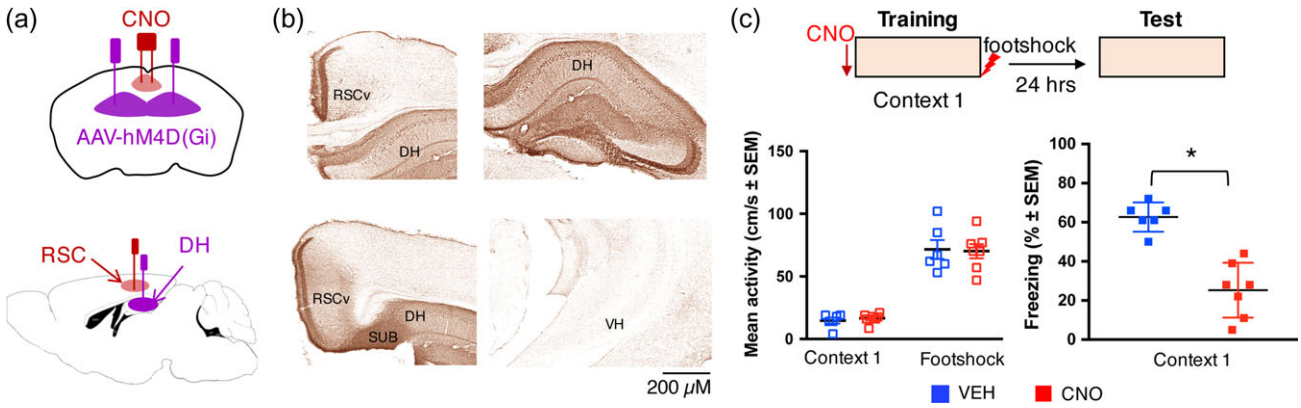

Figure 1. Chemogenetic silencing of DH→ RSC terminals impairs memory encoding of CFC. (*a*) Schematic of virus infusions and cannula implantations. The Cre-independent viral vector AAV-hM4D(Gi)-mCherry was injected into the DH 6 weeks before behavioral experiments. During the same surgery, cannulae were implanted into the RSC bilaterally. (*b*) Immunostaining for mCherry showing expression of hM4D(Gi) in DH and its projection throughout ventral RSC (RSCv) but not in ventral hippocampus (VH). (*c*) Effect of pretraining infusion of CNO on activity (cm/s) during context and shock exposure at training (left) and freezing during context test (right). Pretraining infusions of Veh and CNO did not affect locomotor activity (Veh: 14.7 ± 2.33; CNO: 16.6 ± 1.48) or activity burst (Veh: 71.5 ± 7.52; CNO: 70.1 ± 5.69) to the footshock (activity before shock: $t = 0.71$, $P = 0.49$; activity during shock: $t = 0.15$, $P = 0.89$; Veh $n = 6$, CNO $n = 7$). However, CNO significantly impaired freezing at test when compared to vehicle (Veh)-injected controls ($t = 5.843$, P 0.001; Veh: 62.3 ± 3.03; CNO: 25.3 ± 5.30).

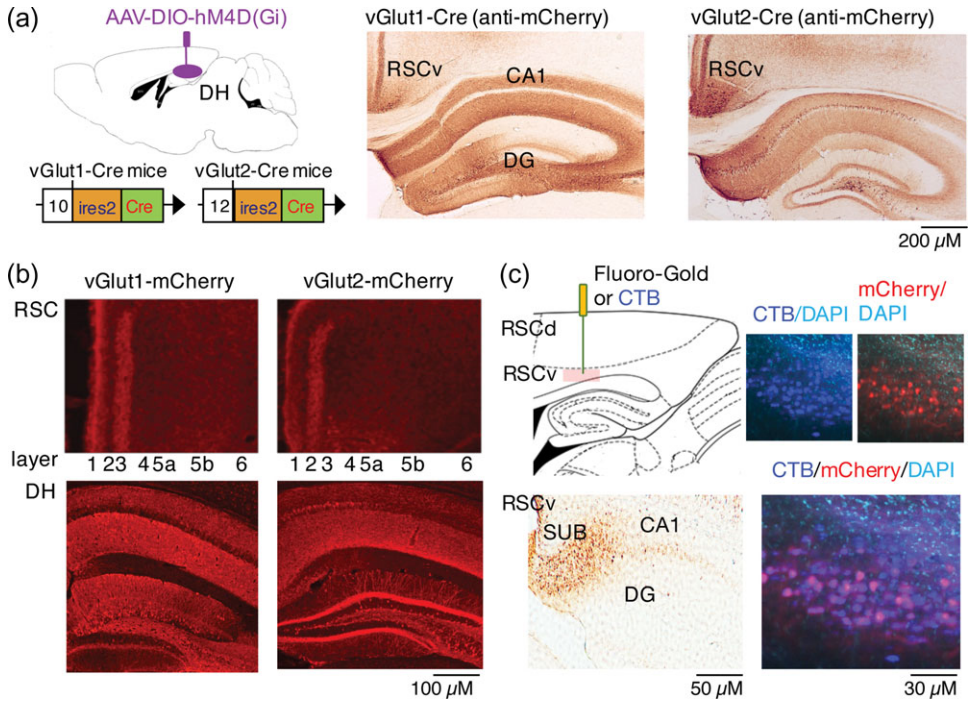

Figure 2. 2 populations of vGlut1$^+$ and vGlut2$^+$ DH neurons project to RSC. (*a*) Schematic of Cre-dependent AAV-DIO-hM4D(Gi)-mCherry infusion in DH of vGlut1-Cre and vGlut2-Cre mice (left). Labeling of vGlut1$^+$ (middle) and vGlut2$^+$ (right) DH neurons 6 weeks after virus expression. The mCherry labeling patterns were similar to the one of endogenous transporters (Supplementary Fig. 2). (*b*) Immunofluorescent staining for mCherry RSC (top) in vGlut1-Cre mice and vGlut2-Cre mice revealing terminal fields in RSC layers 1 and 3. Immunostaining in DH is shown below. (*c*) Retrograde labeling of DH neurons projecting to RSC using Fluoro-Gold (top and bottom left) or CTB (top and bottom right). Fluoro-Gold injected into RSC (top left) was detected predominantly in the subiculum (SUB, bottom left). Sparse signals were also found in dorsomedial CA1. Similarly, injection of CTB (blue) in RSC labels SUB neurons of vGlut1-Cre mice expressing Cre-dependent retrograde AAV-flex-dtTomato (red) (bottom left).

hM4D(Gi) (Zhu et al. 2014; Jovasevic et al. 2015). We expressed the hM4D(Gi) construct in DH neurons, including those that are the source of axonal projections to RSC, by bilaterally infusing AAV-hSyn-HA-hM4D(Gi)-mCherry into DH (Fig. 1*a*). To suppress activity specifically in the DH→RSC circuit, we focally delivered CNO into RSC bilaterally via cannula (Fig. 1*a*). Thus applied, CNO locally blocks presynaptic release from hM4D(Gi)-expressing axon terminals, without affecting the spiking activity of the labeled neurons (Stachniak et al. 2014). Immunohistochemical amplification of the mCherry signal confirmed that prominent hM4D(Gi) expression in RSC axons originate from DH and no viral spread into ventral hippocampus (Fig. 1*b*). After virus expression, we injected 0.2 µl/site of CNO solution (0.3 µg/µL) into RSC 30 min before CFC to silence DH axonal outputs to RSC neurons during memory encoding (Fig. 1*c*). The selection of virus expression and drug infusion times and doses was based on control experiments (Supplementary Fig. 1a–c). During training, CNO did not adversely affect gross sensory-motor function or activity during context exploration or in response to footshock (Fig. 1*c*). At test however, CNO-injected mice froze less than vehicle-injected controls, demonstrating an important contribution of DH→RSC inputs to the encoding of context memory.

Projections from DH to RSC are Molecularly Distinct

Our next goal was to identify the molecular identity of glutamatergic DH→RSC projections. Cortical and thalamic excitatory inputs to RSC have been distinguished by the presence of the vesicular glutamate transporters vGlut1 and vGlut2, respectively (Ichinohe et al. 2008). Because hippocampal neurons are mostly vGlut1$^+$ (Fremeau et al. 2001; Herzog et al. 2006), we hypothesized that DH→RSC projections would mainly express vGlut1. To test this, we used genetically modified mice expressing Cre recombinase driven by the vGlut1 (vGlut1-Cre mice) (Harris et al. 2014) or vGlut2 (vGlut2-Cre mice) (Vong et al. 2011) promoter (Fig. 2*a*), and infused a Cre-dependent AAV-hSyn-DIO-hM4D(Gi)-mCherry bilaterally into DH to restrict hM4D(Gi)-mCherry expression to vGlut1$^+$ or vGlut2$^+$ neurons. The patterns of mCherry expression in DH in both mouse lines were generally similar to those seen with anti-vGlut1 and anti-vGlut2 antibodies in wild-type mice (Supplementary Fig. 2a). Surprisingly, not only vGlut1$^+$, but also vGlut2$^+$ neurons sent dense projections to the ventral RSC (Fig. 2*b*) predominantly in layer 3, but also in layer 1. To determine the origin of DH→RSC projections, we performed retrograde labeling using Fluoro-Gold or Cholera Toxin B (CTB) and found, consistent with earlier work (Wyss and Van Groen 1992; Van Groen and Wyss 2003) that most signals were localized in the subiculum (SUB), which contains both vGlut1$^+$ and vGlut2$^+$ neuronal populations (Supplementary Fig. 2–4).

We next performed experiments in slices (Fig. 3*a*,*b*) to determine the firing patterns of subicular vGlut1$^+$ and vGlut2$^+$ neurons projecting to RSC. Both neurons exhibited burst firing in response to depolarizing current injection at rheobase, the degree of which was significantly greater for vGlut2$^+$ neurons (Fig. 3*c*,*d*). To examine colocalization of vGlut1$^+$ and vGlut2$^+$ neurons, immunostaining for mCherry (indicating vGlut1) and vGlut2 was performed in DH slices from vGlut1-Cre mice injected with Cre-dependent hM4D(Gi)-mCherry. This did not reveal co-immunolabeling (Supplementary Fig. 2b), consistent with earlier evidence for nonoverlapping distribution of vGlut1 and vGlut2 (Heise et al. 2016), and demonstrating that these 2 populations of excitatory subicular neurons project onto the same superficial layers of RSC. Overall, projection from vGlut1$^+$ and vGlut2$^+$ neurons labeled by infusing virus with cannula into DH (Supplementary Fig. 3) or with glass pipette into SUB (Supplementary Fig. 4) showed similar patterns, except for indicated thalamic nuclei. With respect to entorhinal cortex, both applications showed strong vGlut1$^+$ but relatively weak vGlut2$^+$ positive terminal fields.

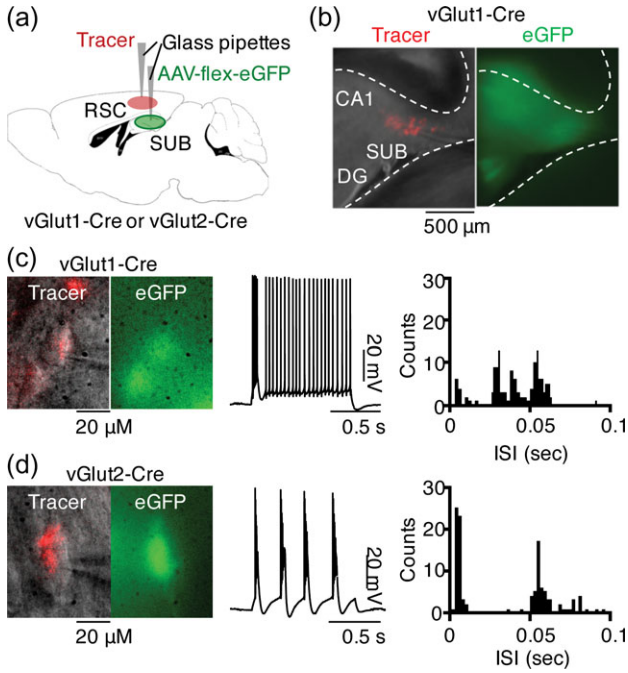

Figure 3. Firing pattern of vGlut1$^+$ and vGlut2$^+$ RSC-projecting neurons in the dorsal SUB. (*a*) Schematic of injections. Retrograde tracer was injected into RSC and AAV-flex-eGFP was injected into SUB of either vGlut1- or vGlut2-cre mice. (*b*) Epifluorescence image showing a population of SUB neurons labeled with tracer (left) and eGFP (right). (*c*) An example bright-field (left) and epifluorescence (right) image of recorded SUB neuron labeled with tracer and eGFP in vGlut1-cre mouse. Typical firing pattern of vGlut1-positive RSC-projecting neuron is also shown (middle). Interspike interval (ISI) histogram of threshold response shown by vGlut1-positive RSC-projecting neurons (right). (*d*) Same as (*c*), but in vGlut2-Cre mouse. Kolmogorov–Smirnov (KS) test comparing ISI distributions showed a significant difference (KS test, $P < 0.001$, vGlut1$^+$ $n = 6$, and vGlut2$^+$ $n = 8$ neurons).

vGlut2$^+$ RSC-Projecting Neurons in the Dorsal SUB Generate More Feedforward Inhibition than vGlut1$^+$ Neurons

We next tested the circuit mechanisms by which DH inputs influence RSC activity, focusing on direct excitation of pyramidal neurons and their feedforward inhibition through the recruitment of local inhibitory neurons. We used slice-based electrophysiology combined with optogenetics. AAV-DIO-hChR2-EYFP was injected into DH of vGlut1- or vGlut2-Cre mice, and slices containing RSC were prepared 3–5 weeks later (Fig. 4*a*, top). In slices from both mice, strong labeling of EYFP-expressing SUB axons was observed in layer 3 of RSC (Fig. 4*a*, bottom), consistent with the projection pattern of vGlut1$^+$ and vGlut2$^+$ DH axons labeled with hM4D(Gi)-mCherry (Fig. 2*b*). We next performed whole-cell recordings of pyramidal neurons in different layers within the same slices, and photostimulated ChR2-expressing vGlut1$^+$ or vGlut2$^+$ SUB axons. In each neuron, we sampled the photo-evoked EPSC and IPSC (Fig. 4*b*–*e*). In RSC slices from vGlut1-Cre mice, stimulation of vGlut1$^+$ SUB axons generated significantly larger EPSC and IPSC in neurons in

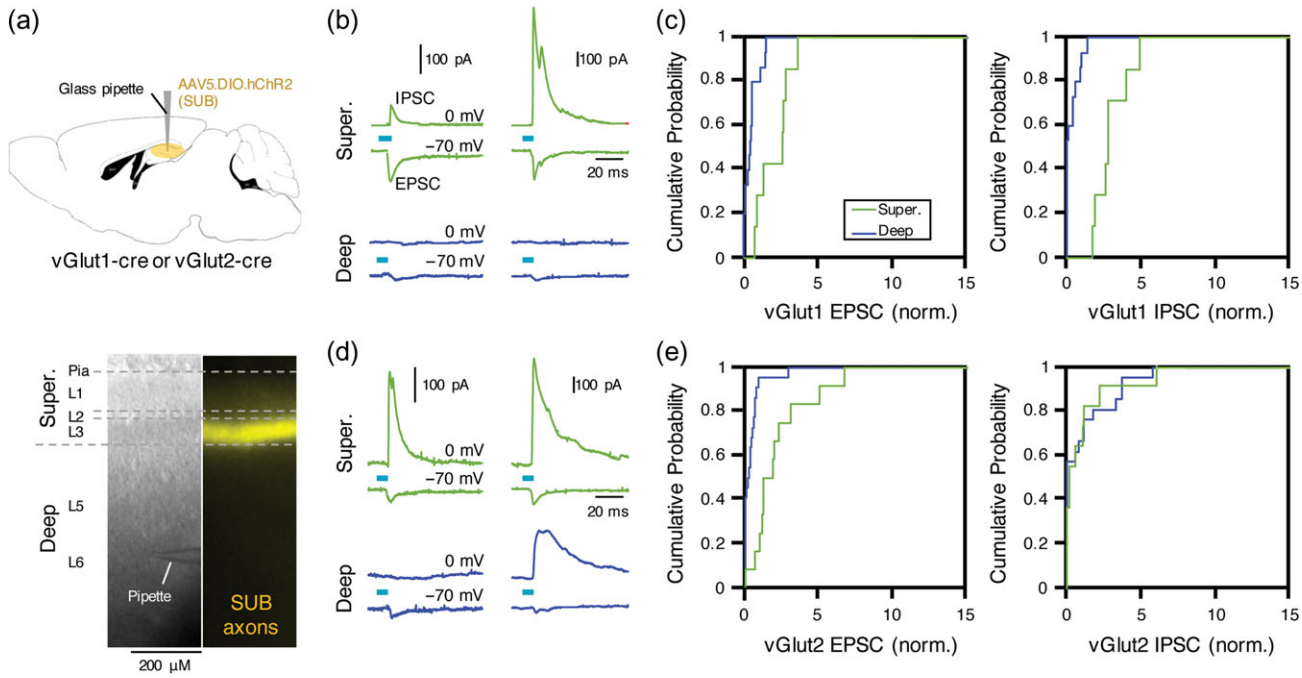

Figure 4. vGlut2$^+$ RSC-projecting neurons in the dorsal SUB generate more feedforward inhibition than vGlut1$^+$ neurons. (*a*) Schematic of injection performed. AAV-DIO-hChR2 was injected into subiculum of either vGlut1- or vGlut2-cre mice (top). Example bright-field and epifluorescence images of RSC slice prepared from vGlut1-cre mouse. Laminar borders are indicated with dotted line (bottom). Layers are further divided into superficial and deep layers. SUB, subiculum. (*b*) EPSC and IPSC recorded from pyramidal neurons in superficial (green) and deep layers of RSC in slice from vGlut1-Cre mice. Traces from 2 neurons are shown (left and right). (*c*) Cumulative distribution histogram of normalized EPSC (left) and IPSC (right) evoked by stimulating vGlut1-positive subicular axons. Each input was normalized to average input recorded from all neurons in same slice. EPSC to superficial (2.1 ± 0.36) versus deep (0.47 ± 0.16): $P < 0.01$, Kolmogorov–Smirnov (KS), $n = 7$ and 15, 4 slices. IPSC to superficial (2.9 ± 0.37) versus deep (0.32 ± 0.15): $P = 0.001$, k–s, $n = 7$ and 15, 4 slices. (*d*) Same as (b), but from vGlut2-Cre mice. (*e*) Same as (c), but for EPSC and IPSC evoked by stimulating vGlut2-positive subicular axons. EPSC to superficial (2.2 ± 0.65) versus deep (0.39 ± 0.21): $P = 0.001$, KS test, $n = 12$ superficial and 22 deep neurons, 6 slices. IPSC to superficial (0.9 ± 0.58) versus deep (1.05 ± 0.56): $P = 0.46$, KS test, $n = 12$ and 21 neurons, 6 slices.

superficial layers relative to neurons in deep layers (Fig. 4*b*,*c*). When this experiment was repeated with RSC slices from vGlut2-Cre mice, photostimulation of vGlut2$^+$ SUB axons evoked greater EPSC in pyramidal neurons in superficial layers relative to deep layers (Fig. 4*d*,*e*), similar to the excitation pattern generated by stimulation of vGlut1$^+$ SUB axons (Fig. 4*c*). In contrast, IPSC generated through vGlut2$^+$ SUB axons were highly variable between superficial and deep layers, with some neurons in both layers receiving IPSC and some receiving weak to no IPSC (Fig. 4*d*,*e*).

These results show that in RSC, both vGlut1$^+$ and vGlut2$^+$ SUB axons strongly excite pyramidal neurons in superficial layers as well as local interneurons that regulate their activity through feedforward inhibition. vGlut2$^+$ SUB axons additionally recruit local interneurons that provide feedforward inhibition onto excitatory neurons in deep layers.

Chemogenetic Silencing of vGlut1$^+$ and vGlut2$^+$ DH→RSC Terminals Differentially Affects Encoding, Consolidation, and Retrieval of CFC

Given the different effects of vGlut1$^+$ and vGlut2$^+$ DH→RSC terminals on RSC excitability, we next sought to determine whether these projections play similar or unique roles in the processing of hippocampus-dependent associative memories. In the first series of experiments, we examined the roles of vGlut1$^+$ and vGlut2$^+$ DH→RSC projections in CFC. We used vGlut1- and vGlut2-Cre mice and Cre-dependent virus to restrict hM4D(Gi) expression to vGlut1$^+$ or vGlut2$^+$ DH neurons. Effectiveness of CNO in reducing photo-evoked synaptic transmission from both vGlut1$^+$ and vGlut2$^+$ DH→RSC axon terminals expressing hM4D(Gi) was confirmed *in vitro*, by co-expressing ChR2 in the same axons and bath-applying CNO while recording photostimulation-evoked responses from postsynaptic RSC neurons (Supplementary Fig. 5a–c). These control experiments showed potent CNO silencing of SUB→RSC synaptic transmission when either vGlut1 or vGlut2 axons co-expressed ChR2 and hM4D(Gi) (Supplementary Fig. 5b–d), but no effect of CNO on evoked responses when axons expressed only ChR2 and not hM4D(Gi) (Supplementary Fig. 5e–g). Inactivation of DH axon terminals in RSC by CNO infusion before conditioning significantly impaired freezing in vGlut1-Cre, but not vGlut2-Cre mice tested 24 h later (Fig. 5*a*). We also examined the effect of the same circuit manipulation on lasting memory consolidation by measuring freezing behavior 24 h and 35 days after CFC. Inactivation of the vGlut1$^+$ pathway caused persistent freezing deficits during both recent and remote memory tests (Fig. 5*b*), indicating silencing of vGlut1$^+$ terminals impairs encoding of context memory.

Interestingly, inactivation of the vGlut2$^+$ pathway, despite not affecting freezing during the recent memory test, resulted in significant freezing impairments during the remote memory test (Fig. 5*b*). Thus, activity of vGlut2$^+$ DH→RSC projections during encoding appears to be important for later context memory consolidation. Possibly, this pathway provides a putative early signal ("tagging") to cortical neurons needed for systems consolidation of memory (Lesburgueres et al. 2011; Kitamura et al. 2017). We next studied whether vGlut1$^+$ and vGlut2$^+$ DH inputs to RSC contribute to memory retrieval. Local silencing of vGlut1$^+$ DH terminals in RSC before the test for recent but not remote memory impaired freezing (Fig. 5*c*). In contrast, local

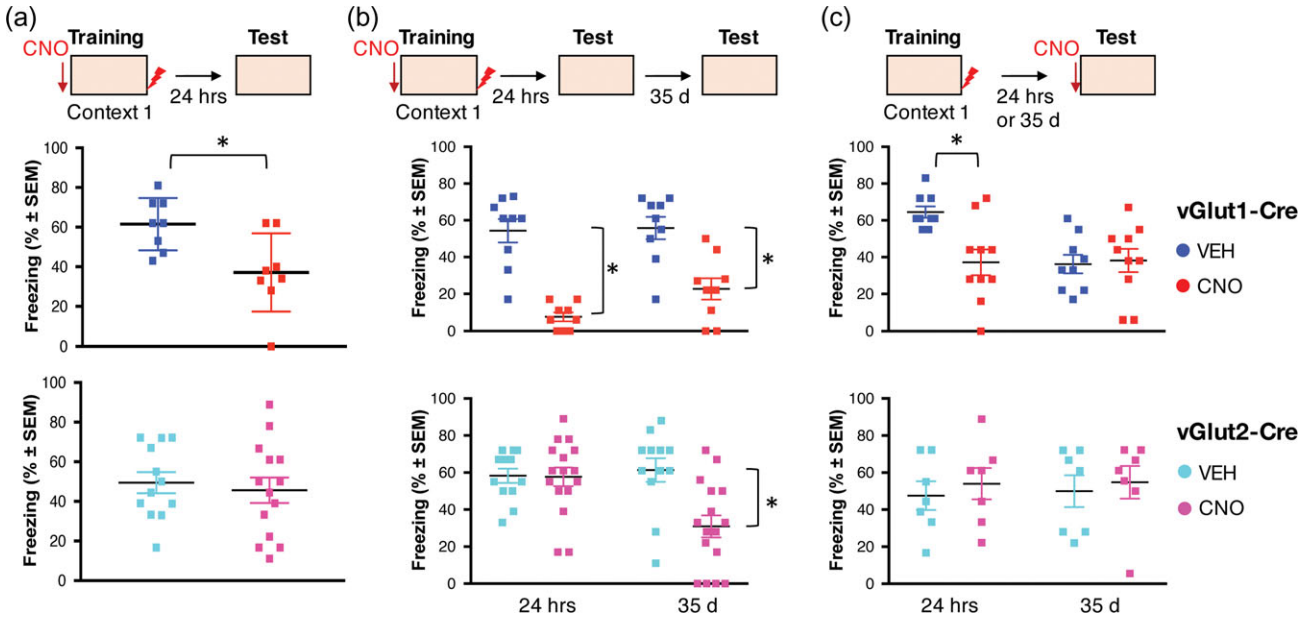

Figure 5. Chemogenetic silencing of vGlut1$^+$ DH→ RSC terminals impair encoding and retrieval of contextual fear conditioning. (*a*) Experimental design similar to Figure 1 except for infusion of a Cre-dependent AAV8-DIO-hM4D(Gi)-mCherry. Freezing during the context test was significantly reduced in vGlut1-Cre mice injected with CNO when compared to Veh (Veh: 61.5 ± 4.68; CNO: 37.13 ± 6.99; $t = 2.87$, $P < 0.05$ ($n = 8$/group)), but not in vGlut2-Cre mice (Veh: 49.48 ± 5.32; CNO: 45.66 ± 6.41; $t = 0.45$, $P = 0.65$; Veh $n = 12$, CNO $n = 14$). (*b*) Within-subject design was used to determine the effect of pretraining CNO on recent and remote memory. Significant treatment effects were found for each genotype (vGlut1-Cre: $F_{1,16} = 43.78$, $P < 0.001$; $n = 9$/group; vGlut2-Cre: $F_{1,16} = 10.91$, $P < 0.01$; Veh $n = 12$, CNO $n = 14$). However, vGlut1-Cre mice receiving CNO before training showed reduced freezing both at recent (Veh: 54.3 ± 6.36; CNO: 7.56 ± 2.29; $P < 0.05$) and remote memory tests (Veh: 55.8 ± 6.09; CNO: 22.7 ± 5.79; $P < 0.01$), whereas similarly treated vGlut2-Cre mice showed freezing deficits only at the remote (Veh: 61.3 ± 6.35; CNO: 30.9 ± 5.96; $P < 0.01$), but not recent test (Veh: 58.2 ± 3.86; CNO: 57.7 ± 5.06). (*c*) Infusion of CNO before the recent memory test impaired freezing to the conditioning context in vGlut1-Cre mice (Veh: 64.6 ± 3.08; CNO: 37.2 ± 6.98; $t = 3.14$, $P < 0.01$; $n = 9$/group) without affecting freezing in vGlut2-Cre mice (Veh: 47.5 ± 7.73; CNO: 53.9 ± 8.46; $t = 0.56$, $P = 0.58$; $n = 7$/group). Infusion of CNO before the remote memory test was ineffective in either mouse line (vGlut1-Cre, Veh: 36.2 ± 5.04; CNO: 38.2 ± 6.32; $t = 0.61$, $P = 0.54$; $n = 15$/group; vGlut2-Cre: Veh: 49.9 ± 8.62; CNO: 54.8 ± 8.78; $t_{13} = 0.39$, $P = 0.7$; $n = 7$/group).

silencing of vGlut2$^+$ DH terminals had no effect on either recent or remote memory retrieval (Fig. 5c).

Together, these findings reveal a key role of vGlut1$^+$ DH→RSC projections in the processing of recent context memories as well as a contribution of vGlut2$^+$ DH→RSC projections to systems consolidation of context memories.

Discussion

By combining optogenetic, chemogenetic, and behavioral analyses, we delineate vGlut1$^+$ and vGlut2$^+$ DH→RSC circuits that play distinct roles in the processing of contextual associative memories. Encoding and retrieval of recent context memories required vGlut1$^+$ afferents, with vGlut2$^+$ afferents contributing to the systems consolidation and persistence of these memories.

Interestingly, although DH receives vGlut1$^+$ and vGlut2$^+$ presynaptic terminals from different sources [vGlut1$^+$ presynaptic terminals from the trisynaptic hippocampal circuit and from the cortex (Balschun et al. 2010; Zander et al. 2010) and vGlut2$^+$ presynaptic terminals from the supramamillary nucleus or hillar mossy cells (Halasy et al. 2004; Boulland et al. 2009)], DH neurons send both vGlut1$^+$ and vGlut2$^+$ projections to RSC. The importance of this overlap is revealed by the synergistic contribution of these projections to the formation and persistence of fear-inducing context memories.

The distinct contribution of vGlut1$^+$ and vGlut2$^+$ DH→RSC projections to memory processing is not surprising given the known differences between vGlut1$^+$ and vGlut2$^+$ synapses in probability of transmitter release and synaptic plasticity (Fremeau et al. 2004; Boulland et al. 2009). Here we show that these synapses also exert different effects at the level of cellular circuits. Namely, vGlut1$^+$ and vGlut2$^+$pathways arose from presynaptic neurons with distinct burst-firing properties, which furnished monosynaptic excitation to RSC excitatory neurons in a similar way, preferentially innervating superficial- rather than deep-layer pyramidal neurons. However, feedforward (disynaptic) inhibition, while similarly restricted to pyramidal neurons in superficial layers when triggered by vGlut1$^+$ DH terminals, was detected in both superficial- and deep-layer RSC pyramidal neurons when triggered by vGlut2$^+$ DH terminals. These similarities and differences are consistent with, and likely contribute to the distinct roles of vGlut1$^+$ and vGlut2$^+$ pathways in the formation and persistence of stress-related context memories.

Consistent with our findings with recent context memory, haploinsufficiency of vGlut1, but not vGlut2, impairs learning and memory (Callaerts-Vegh et al. 2013). Although developmental effects of vGlut2 have been reported, dysfunction of this transporter is accompanied by down-regulation of vGlut1 as well (He et al. 2012), so the individual roles of vGlut1$^+$ and vGlut2$^+$ pathways could not be dissected with genetic tools. Chemogenetic silencing, however, identified a discrete role of vGlut2$^+$ DH→RSC pathways in the persistence of fear-inducing context memories. Importantly, early silencing of vGlut2$^+$ terminals during memory encoding was required for disruption of later consolidation, but the same manipulation was ineffective during retrieval of remote memory. These findings are in line with the time-limited role of DH in context memory encoding (Kim and Fanselow 1992), and with previous observations showing that hippocampal input to the neocortex during early

stages of memory encoding is needed for latter systems consolidation of that memory (Lesburgueres et al. 2011; Kitamura et al. 2017). The molecular basis of this phenomenon is not known beyond a hypothetical memory "tag", however, our findings provide initial indication that such tag might be provided to the neocortex by vGlut2$^+$ terminals.

Our findings support the view that at least a subset of DH neuronal populations engaged in encoding also contributes to retrieval of recent memories (Reijmers et al. 2007; Tonegawa et al. 2015) without playing a major role in retrieval of remote memories (Kitamura et al. 2017). It should be mentioned, however, that this view was recently challenged by findings demonstrating differential involvements of CA1- versus and SUB-entorhinal cortical projections in context memory encoding and retrieval, respectively (Roy et al. 2017). While we cannot rule out such possibility, given that our virus infusions targeted the entire DH, a similar scenario is not very likely because CA1 DH→RSC projections were very scarce.

It was recently reported that RSC is not involved in systems consolidation of memory downstream of the DH-entorhinal cortical circuit (Kitamura et al. 2017). It can be speculated, based on the known RSC connectome (Vogt and Laureys 2005; Sugar et al. 2011), that RSC contributes to neocortical mechanisms of memory either upstream of the entorhinal cortex (through a DH-RSC- entorhinal cortex circuit) or through a parallel RSC-anterior cingulate cortex circuit (Shibata et al. 2004). If so, these different DH-neocortical circuits could provide an opportunity for different treatment approaches for memory-related disorders.

Supplementary Material

Supplementary material is available at *Cerebral Cortex* online.

Authors' Contributions

J.R. designed the behavioral experiments. N.Y. and G.S. designed and N.Y. conducted the *in vitro* electrophysiological experiments. K.C., J.K., and A.G. conducted the behavioral experiments and the histology. N.Y. and A.G. conducted the tract-tracing studies; N.Y., K.C., and J.R. analyzed the data. J.R. and G.S. secured the funding. N.Y., G.S., and J.R. wrote the manuscript. All authors discussed and commented on the manuscript.

Funding

This work was funded by NIMH grants to J.R. (MH108837 and MH078064) and NINDS grant to G.S. (NS061963).

Notes

We thank Hongkui Zeng (Allen Brain Institute) for feedback on the breeding, genotyping, and overall characterization of vGlut1-Cre mice. Undergraduate students Jinhak Kim, Gabriel Hast, and Helen Chen for their help with the maintenance of mouse lines and animal surgery and care. *Conflict of Interest*: None declared.

References

Aggleton JP. 2010. Understanding retrosplenial amnesia: insights from animal studies. Neuropsychologia. 48:2328–2338.

Apicella AJ, Wickersham IR, Seung HS, Shepherd GM. 2012. Laminarly orthogonal excitation of fast-spiking and low-threshold-spiking interneurons in mouse motor cortex. J Neurosci. 32:7021–7033.

Balschun D, Moechars D, Callaerts-Vegh Z, Vermaercke B, Van Acker N, Andries L, D'Hooge R. 2010. Vesicular glutamate transporter VGLUT1 has a role in hippocampal long-term potentiation and spatial reversal learning. Cereb Cortex. 20: 684–693.

Blanchard RJ, Blanchard DC. 1969. Crouching as an index of fear. J Comp Physiol Psychol. 67:370–375.

Boulland JL, Jenstad M, Boekel AJ, Wouterlood FG, Edwards RH, Storm-Mathisen J, Chaudhry FA. 2009. Vesicular glutamate and GABA transporters sort to distinct sets of vesicles in a population of presynaptic terminals. Cereb Cortex. 19:241–248.

Callaerts-Vegh Z, Moechars D, Van Acker N, Daneels G, Goris I, Leo S, Naert A, Meert T, Balschun D, D'Hooge R. 2013. Haploinsufficiency of VGluT1 but not VGluT2 impairs extinction of spatial preference and response suppression. Behav Brain Res. 245:13–21.

Cenquizca LA, Swanson LW. 2007. Spatial organization of direct hippocampal field CA1 axonal projections to the rest of the cerebral cortex. Brain Res Rev. 56:1–26.

Corcoran KA, Donnan MD, Tronson NC, Guzman YF, Gao C, Jovasevic V, Guedea AL, Radulovic J. 2011. NMDA receptors in retrosplenial cortex are necessary for retrieval of recent and remote context fear memory. J Neurosci. 31:11655–11659.

Cowansage KK, Shuman T, Dillingham BC, Chang A, Golshani P, Mayford M. 2014. Direct reactivation of a coherent neocortical memory of context. Neuron. 84:432–441.

Fanselow MS. 1990. Factors governing one-trial contextual conditioning. Anim Learn Behav. 18:264–270.

Frankland PW, Bontempi B, Talton LE, Kaczmarek L, Silva AJ. 2004. The involvement of the anterior cingulate cortex in remote contextual fear memory. Science. 304:881–883.

Fremeau RT Jr., Kam K, Qureshi T, Johnson J, Copenhagen DR, Storm-Mathisen J, Chaudhry FA, Nicoll RA, Edwards RH. 2004. Vesicular glutamate transporters 1 and 2 target to functionally distinct synaptic release sites. Science. 304: 1815–1819.

Fremeau RT Jr., Troyer MD, Pahner I, Nygaard GO, Tran CH, Reimer RJ, Bellocchio EE, Fortin D, Storm-Mathisen J, Edwards RH. 2001. The expression of vesicular glutamate transporters defines two classes of excitatory synapse. Neuron. 31:247–260.

Gao C, Gill MB, Tronson NC, Guedea AL, Guzman YF, Huh KH, Corcoran KA, Swanson GT, Radulovic J. 2010. Hippocampal NMDA receptor subunits differentially regulate fear memory formation and neuronal signal propagation. Hippocampus. 20:1072–1082.

Halasy K, Hajszan T, Kovacs EG, Lam TT, Leranth C. 2004. Distribution and origin of vesicular glutamate transporter 2-immunoreactive fibers in the rat hippocampus. Hippocampus. 14:908–918.

Harris JA, Hirokawa KE, Sorensen SA, Gu H, Mills M, Ng LL, Bohn P, Mortrud M, Ouellette B, Kidney J, et al. 2014. Anatomical characterization of Cre driver mice for neural circuit mapping and manipulation. Front Neural Circuits. 8: 76.

He H, Mahnke AH, Doyle S, Fan N, Wang CC, Hall BJ, Tang YP, Inglis FM, Chen C, Erickson JD. 2012. Neurodevelopmental role for VGLUT2 in pyramidal neuron plasticity, dendritic refinement, and in spatial learning. J Neurosci. 32: 15886–15901.

Heise C, Schroeder JC, Schoen M, Halbedl S, Reim D, Woelfle S, Kreutz MR, Schmeisser MJ, Boeckers TM. 2016. Selective

Localization of Shanks to VGLUT1-Positive Excitatory Synapses in the Mouse Hippocampus. Front Cell Neurosci. 10:106.

Herzog E, Takamori S, Jahn R, Brose N, Wojcik SM. 2006. Synaptic and vesicular co-localization of the glutamate transporters VGLUT1 and VGLUT2 in the mouse hippocampus. J Neurochem. 99:1011–1018.

Ichinohe N, Knight A, Ogawa M, Ohshima T, Mikoshiba K, Yoshihara Y, Terashima T, Rockland KS. 2008. Unusual patch-matrix organization in the retrosplenial cortex of the reeler mouse and Shaking rat Kawasaki. Cereb Cortex. 18: 1125–1138.

Jovasevic V, Corcoran KA, Leaderbrand K, Yamawaki N, Guedea AL, Chen HJ, Shepherd GM, Radulovic J. 2015. GABAergic mechanisms regulated by miR-33 encode state-dependent fear. Nat Neurosci. 18:1265–1271.

Keene CS, Bucci DJ. 2008. Contributions of the retrosplenial and posterior parietal cortices to cue-specific and contextual fear conditioning. Behav Neurosci. 122:89–97.

Kim JJ, Fanselow MS. 1992. Modality-specific retrograde amnesia of fear. Science. 256:675–677.

Kitamura T, Ogawa SK, Roy DS, Okuyama T, Morrissey MD, Smith LM, Redondo RL, Tonegawa S. 2017. Engrams and circuits crucial for systems consolidation of a memory. Science. 356:73–78.

Kwapis JL, Jarome TJ, Lee JL, Gilmartin MR, Helmstetter FJ. 2014. Extinguishing trace fear engages the retrosplenial cortex rather than the amygdala. Neurobiol Learn Mem. 113:41–54.

Lesburgueres E, Gobbo OL, Alaux-Cantin S, Hambucken A, Trifilieff P, Bontempi B. 2011. Early tagging of cortical networks is required for the formation of enduring associative memory. Science. 331:924–928.

Reijmers LG, Perkins BL, Matsuo N, Mayford M. 2007. Localization of a stable neural correlate of associative memory. Science. 317:1230–1233.

Roy DS, Kitamura T, Okuyama T, Ogawa SK, Sun C, Obata Y, Yoshiki A, Tonegawa S. 2017. Distinct neural circuits for the formation and retrieval of episodic memories. Cell. 170: 1000–1012 e1019.

Shibata H, Kondo S, Naito J. 2004. Organization of retrosplenial cortical projections to the anterior cingulate, motor, and prefrontal cortices in the rat. Neurosci Res. 49:1–11.

Squire LR, Alvarez P. 1995. Retrograde amnesia and memory consolidation: a neurobiological perspective. Curr Opin Neurobiol. 5:169–177.

Stachniak TJ, Ghosh A, Sternson SM. 2014. Chemogenetic synaptic silencing of neural circuits localizes a hypothalamus—midbrain pathway for feeding behavior. Neuron. 82:797–808.

Sugar J, Witter MP, van Strien NM, Cappaert NL. 2011. The retrosplenial cortex: intrinsic connectivity and connections with the (para)hippocampal region in the rat. An interactive connectome. Front Neuroinform. 5:7.

Suter BA, O'Connor T, Iyer V, Petreanu LT, Hooks BM, Kiritani T, Svoboda K, Shepherd GM. 2010. Ephus: multipurpose data acquisition software for neuroscience experiments. Front Neural Circuits. 4:100.

Tonegawa S, Pignatelli M, Roy DS, Ryan TJ. 2015. Memory engram storage and retrieval. Curr Opin Neurobiol. 35: 101–109.

Van Groen T, Wyss JM. 2003. Connections of the retrosplenial granular b cortex in the rat. J Comp Neurol. 463:249–263.

Vogt BA, Laureys S. 2005. Posterior cingulate, precuneal and retrosplenial cortices: cytology and components of the neural network correlates of consciousness. Prog Brain Res. 150:205–217.

Vong L, Ye C, Yang Z, Choi B, Chua S Jr., Lowell BB. 2011. Leptin action on GABAergic neurons prevents obesity and reduces inhibitory tone to POMC neurons. Neuron. 71:142–154.

Wiltgen BJ, Tanaka KZ. 2013. Systems consolidation and the content of memory. Neurobiol Learn Mem. 106:365–371.

Wyss JM, Van Groen T. 1992. Connections between the retrosplenial cortex and the hippocampal formation in the rat: a review. Hippocampus. 2:1–11.

Xue M, Atallah BV, Scanziani M. 2014. Equalizing excitation–inhibition ratios across visual cortical neurons. Nature. 511: 596–600.

Zander JF, Munster-Wandowski A, Brunk I, Pahner I, Gomez-Lira G, Heinemann U, Gutierrez R, Laube G, Ahnert-Hilger G. 2010. Synaptic and vesicular coexistence of VGLUT and VGAT in selected excitatory and inhibitory synapses. J Neurosci. 30: 7634–7645.

Zhu H, Pleil KE, Urban DJ, Moy SS, Kash TL, Roth BL. 2014. Chemogenetic inactivation of ventral hippocampal glutamatergic neurons disrupts consolidation of contextual fear memory. Neuropsychopharmacology. 39:1880–1892.